THE JOURNAL OF PHYSICAL CHEMISTRY B

Article

pubs.acs.org/JPCB

Calcium-43 NMR Studies of Polymorphic Transition of Calcite to Aragonite

Yu-Chieh Huang,[†] Yun Mou,[†] Tim Wen-Tin Tsai,[†] Yu-Ju Wu,[†] Hsin-Kuan Lee,[†] Shing-Jong Huang,*[,‡] and Jerry C. C. Chan*[,†]

[†]Department of Chemistry, and [‡]Instrumentation Center, National Taiwan University, No. 1, Section 4, Roosevelt Road, Taipei 106, Taiwan

Supporting Information

ABSTRACT: Phase transformation between calcite and aragonite is an important issue in biomineralization. To shed more light on the mechanism of this process at the molecular level, we employ solid-state ^{43}Ca NMR to study the phase transformation from calcite to aragonite as regulated by magnesium ions, with ^{43}Ca enrichment at a level of 6%. Using the gas diffusion approach, the phase of Mg-calcite is formed initially and the system subsequently transforms to aragonite as the reaction time proceeds. Our ^{43}Ca solid-state NMR data support the dissolution-recrystallization mechanism for the calcite to aragonite transition. We find that the ^{43}Ca NMR parameters of Mg-calcite are very similar to those of pure calcite. Under the high-resolution condition provided by magic-angle spinning at 4 kHz, we can monitor the variation of the ^{43}Ca NMR parameters of the aragonite signals for the samples obtained at different reaction times. Our data suggest that in the presence of a significant amount of Mg^{2+} ions, aragonite is the most stable polymorph of calcium carbonate. The initial precipitated crystallites of aragonite have spine-like morphology, for which the ^{43}Ca spin−lattice relaxation data indicate that the ions in the lattice have considerable motional dynamics. As the crystallinity of aragonite improves further, the ^{43}Ca T_1 parameter of the aragonite phase changes considerably and becomes very similar to that obtained for pure aragonite. For the first time, the difference in crystal morphologies and crystallinity of the aragonite phase has been traced down to the subtle difference in the motional dynamics at the molecular level.

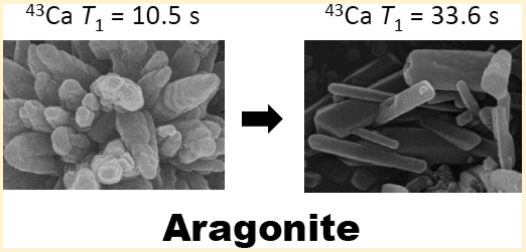

INTRODUCTION

Calcite and aragonite are two important crystalline phases of calcium carbonate in biomineralization.[1,2] The lattice structures of these two polymorphs of calcium carbonate are very similar in the *ab* plane.[3] While the ocean surface waters are supersaturated with respect to both calcite and aragonite, organisms such as calcitic coccolithophoridae and the aragonitic pteropoda are highly selective in the biomineralization of one polymorph or another.[1] How Nature accomplishes the controlled precipitation of calcite and/or aragonite in organisms such as mollusca and echinodermata is a long-standing enigma. To shed more light on this biomineralization process, many in vitro studies of the phase transformation between calcite and aragonite have been carried out. In particular, the effects of Mg^{2+} ions on the crystallization process of calcium carbonate have been extensively studied: (i) in water−alcohol mixture,[4] air−water interface,[5] and nonaqueous environment;[6] (ii) on self-assemble monolayer[7] and inorganic substrate;[8,9] (iii) in the presence of polymer-induced liquid precursor,[10] organic additives,[11−13] and macromolecules.[14] The majority of these works focus on the characterization of the phases and morphologies of the resultant crystallites upon the variation of Mg^{2+} concentration and other relevant experimental parameters. In addition to the large collection of interesting morphologies which exemplify the variety of the crystal habits of biogenic calcium carbonates, magnesian calcites with very high Mg content have been successfully prepared in vitro.

Although powder X-ray diffraction, infrared spectroscopy, and electron microscopy have been extensively employed to characterize the crystallization process in the above studies, the transformation mechanism at the molecular level remains poorly understood. The major difficulty is that these physical techniques are neither element selective nor well suited to probe the structure and motional dynamics at the atomic level. As a powerful complementary technique, ^{43}Ca solid-state NMR (SSNMR) spectroscopy is in principle an ideal option for the study of the crystallization of calcium carbonates. However, due to the low natural abundance and small gyromagnetic ratio of the ^{43}Ca nucleus, application of ^{43}Ca NMR in the field of biomineralization is still in its infancy stage. Nonetheless, the NMR studies of hydroxyapatite,[15−19] bone,[20,21] and polymorphs of calcium carbonate[22] all suggest that ^{43}Ca SSNMR has tremendous potential in the structural elucidation of calcified tissues.[23,24] In particular, Bryce et al. have shown that the ^{43}Ca NMR signals of calcite and aragonite are well resolved.[22] Therefore, ^{43}Ca NMR spectroscopy should be an effective method for the study of the phase transition between

Received: October 8, 2012
Revised: November 16, 2012
Published: November 19, 2012

ACS Publications © 2012 American Chemical Society

calcite and aragonite. Although it has been shown that ^{43}Ca SSNMR is feasible for samples in natural abundance,[15,16,18,20,22,25−31] the sensitivity issue remains a serious concern especially when ultrahigh-field facilities (≥18.8 T) are not available. Consequently, ^{43}Ca enrichment is still advisable, especially when an accurate characterization of the quadrupolar parameters at the calcium sites is desired. We note in passing that the sample amount and hence the cost of enrichment can be greatly reduced with the use of magic-angle-spinning coil, although dedicated hardware is required for its implementation.[32]

In this work, we employ ^{43}Ca SSNMR to study the phase transformation of calcite to aragonite in vitro. To our knowledge, this is the first attempt to exploit ^{43}Ca SSNMR spectroscopy for the study of the phase transformation process of calcium carbonate. We deliberately prepare a simple gas diffusion system to regulate the phase transformation of calcite to aragonite by Mg^{2+} ions, with ^{43}Ca enrichment at a level of 6%. Our ^{43}Ca solid-state NMR data support the dissolution-recrystallization mechanism for the calcite to aragonite transition. We also found that the motional dynamics of the aragonite phase in spine-like and rod-like morphologies are distinctive, as reflected in their difference in the ^{43}Ca spin−lattice relaxation parameters.

MATERIALS AND METHODS

Sample Preparation. ^{43}Ca enriched $CaCO_3$ (60%) was obtained from CortecNet (Tilleuls, France). All other chemicals were obtained from Acros and used as received without further purification. Calcium source was prepared by dissolving 10 mg of ^{43}Ca-labeled $CaCO_3$ and 90 mg of unlabeled $CaCO_3$ in 0.2 mL of concentrated HCl. After complete dissolution, 3 mL of deionized (DI) water was added and the solution was then purged by N_2 gas for 30 min to remove CO_2. After the addition of 0.1015 g of $MgCl_2{\cdot}6H_2O$, the solution was diluted to 10 mL by DI water and the pH was adjusted to 8.4−8.6 using NaOH solution. The Mg/Ca molar ratio of the resultant solution has a nominal value of 0.5, where 6% of the calcium ions are ^{43}Ca enriched unless stated otherwise. Carbonate precipitates were obtained by the CO_2 gas diffusion method at ambient temperature. Briefly, three glass vials containing the ^{43}Ca labeled Mg/Ca solution (10 mL), an unlabeled Mg/Ca solution (10 mL), and 1 g of $(NH_4)_2CO_3$ powder were placed in a two-liter desiccator under reduced pressure (120 Torr), where the Mg/Ca solutions were under continuous stirring. Precipitates were collected after the predestined reaction time by repeat centrifugation (15000*g* for 10 min) and washing with DI water three times. The collected samples were lyophilized and stored in desiccator. For convenience, all of the samples are henceforth referred to by reference to their reaction times, viz., 15 min, 40 min, 2 h, 24 h, and 9 d. The sample of Mg-free calcite was prepared in a similar fashion without the addition of the Mg source and the reaction time was set to 24 h. The ^{43}Ca labeled samples were prepared for the ^{43}Ca NMR measurements. All other characterizations were carried out for the samples in natural abundance.

Characterization. X-ray powder diffraction (XRD) analysis was performed on a Philips X'pert diffractometer, using Cu Kα radiation (λ = 1.5418 Å). The step sizes were set to 0.066845° and 0.008356° for the regular and high-resolution XRD measurements, respectively. Absorbance Fourier-transform infrared (FT-IR) spectra were collected using a Varian 640-IR spectrometer, in the range of 400−4000 cm $^{-1}$. The field emission scanning electron microscopy (FESEM) images were taken on a Hitachi S-4800 field emission scanning electron microscope. The transmission electron microscope (TEM) images and selected-area electron diffraction (SAED) patterns were taken on Hitachi H-7100 and Philips FEI Tecnai 20 G^2 instruments operating at 75 and 200 kV, respectively. The energy dispersive X-ray (EDX) analysis was done on a LEO 1530 field emission scanning electron microscope equipped with EDX accessories. The inductively coupled plasma mass spectrometry (ICP-MS) measurements were performed on an Agilent 7500ce system. The standard solutions of 1000 mg/L Ca^{2+} and Mg^{2+} (Merck) were diluted into ppb levels for the calibration measurements.

Solid-State NMR. All NMR experiments were carried out at ambient temperature on a wide-bore Bruker Avance III spectrometer equipped with a commercial 4 mm probe. ^{43}Ca NMR spectra were measured at 40.1 MHz (14.1 T). ^{43}Ca chemical shifts were externally referenced to a freshly prepared $CaCl_2$ solution of natural abundance (1.0 M). The rf field was set to 27.8 kHz with a pulse width of 2.3 μs, which corresponds to the selective $\pi/2$ excitation for spin 7/2 nuclei. All of the ^{43}Ca magic-angle spinning (MAS) spectra were acquired at a spin rate of 4 kHz. For some of the ^{43}Ca MAS spectra, the method of rotor-assisted population transfer (RAPT) was used to enhance the sensitivity,[33,34] for which a total of 20 RAPT pulses with interpulse delay of 2.5 μs were applied and followed by a selective $\pi/2$ pulse of 9 μs. ^{43}Ca spin−lattice relaxation times of selected samples were characterized by the method of saturation recovery, where the signal was saturated by a train of 40 $\pi/2$ pulses with interpulse delay of 100 ms. Spectral deconvolutions were carried out using DMFit2011.[35]

RESULTS

Phase Transformation of Carbonates. The precipitation process of carbonates is a delicate balance of the kinetic and thermodynamic events. The initial concentrations of the Mg^{2+} and Ca^{2+} ions are 0.05 and 0.1 M, respectively. As NH_3 and CO_2 diffused into the mother liquor, the pH increased to 10 after 15 min and decreased slowly to 9 in a period of 24 h. The amount of precipitation is very limited initially but it becomes more substantial for longer reaction time (Table S1 of the Supporting Information). Figure 1 shows the XRD patterns obtained for the samples with different reaction times and those

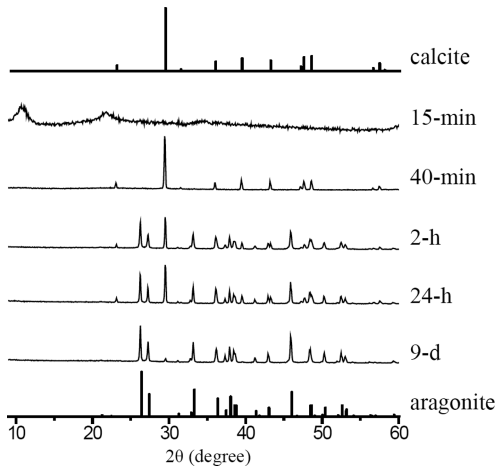

Figure 1. XRD patterns acquired for the sample series.

dx.doi.org/10.1021/jp309923p | J. Phys. Chem. B 2012, 116, 14295−14301

calculated based on the calcite and aragonite structures. It is noteworthy that the 15-min sample is amorphous because there are only three broad humps that appear at 11°, 22°, and 34°. In addition, our pattern is quite different from those reported for amorphous calcium carbonate (ACC), for which the broad humps are near 33° and 46°.[36−38] The XRD pattern of the 40-min sample is quite similar to that of pure calcite (JCPDS 47-1743). Nonetheless, Mg^{2+} ions can be incorporated into the crystal lattice of calcite, resulting in a shift of the diffraction peak of (104). It has been shown that the amount of Mg^{2+} ions can be estimated empirically based on the extent of the peak shift.[11] The corresponding high-resolution XRD patterns of the 2-h and 24-h samples were measured (Figure S1). For the 40-min sample, we find that the diffraction peak is shifted toward the high-angle side compared with that of the Mg-free calcite. Consequently, the 40-min sample can be assigned to Mg-calcite and the Mg^{2+} content is estimated to be 1.6 mol %. For the 2-h sample, both the Mg-calcite and aragonite phases are present. The amount of Mg^{2+} ions in the Mg-calcite phase is determined to be 3.0 mol %. Very similar XRD results were obtained for the 24-h sample. As the reaction proceeds further, the 9-d sample becomes dominated by the aragonite phase (JCPDS 41-1475). Note that Mg^{2+} ions cannot be incorporated into the lattice of aragonite.[4] On the basis of the relative intensities of the (104) peak of calcite and the (111) peak of aragonite, we estimate that 71% of the species are in the aragonite phase and the rest are in the calcitic phase for both the 2-h and 24-h samples.

As an independent characterization of the phase transformation, we also measured the FT-IR spectra of our sample series (Figure 2). To help assign our spectra, we prepared two

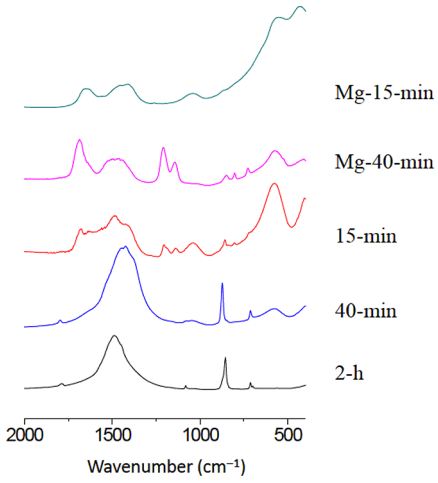

Figure 2. FT-IR spectra obtained for the 40-min, 2-h, and 24-h samples.

control samples, viz., Mg-15-min and Mg-40-min, which were prepared identically as the 15-min and 40-min samples, respectively, except that the Ca source was replaced by $MgCO_3$. We infer from the FT-IR data of the control samples that the IR spectrum of the 15-min sample is overwhelmed by the absorption peaks of the amorphous phase of $Mg(OH)_2$ and/or $MgCO_3$ in its hydrated forms, so that the characteristic absorption peaks of ACC (866 and 1074 cm^{-1}), if any, are not resolved in the 15-min sample. For the 40-min sample, the absorption bands at 1424 (ν_3), 872 (ν_2), and 712 cm^{-1} (ν_4) can be unequivocally assigned to the calcitic phase.[5] It is noteworthy that considerable amount of the amorphous phase is still found in the 40-min sample, as indicated by the broad absorption bands at 1045 and 576 cm^{-1}. The IR spectra of the 2-h and 24-h samples are quite similar, for which both the characteristic peaks of calcite and aragonite are observed. As expected, the spectrum of the 9-d sample is dominated by the absorption bands of aragonite. Overall, the FT-IR results are in good agreement with the XRD data, showing that the system transforms gradually from the calcitic phase to the aragonite phase.

Mg^{2+} Ions Incorporated in Carbonates. To follow the precipitation process of our system, the concentration of the Ca^{2+} and Mg^{2+} ions in the supernatant and the precipitate were monitored by ICP-MS. As shown in Figure 3, the relative

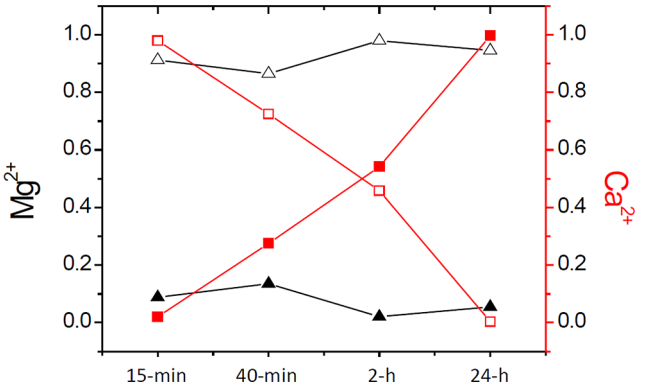

Figure 3. Relative amounts of Mg^{2+} and Ca^{2+} ions in the supernatant and sample precipitate determined by ICP-MS. Triangles and squares denote the data of Mg^{2+} and Ca^{2+} ions, respectively. Filled and open symbols represent the data obtained for the precipitate and the supernatant, respectively.

amount of Ca^{2+} ions in the supernatant decreases monotonically from 98% to less than 0.4% when the reaction time proceeds from 15 min to 24 h. Interestingly, the relative amount of Mg^{2+} ions in the supernatant is 91% at 15 min and 86% at 40 min and increases again to more than 95% afterward. Given that the molar ratio of Mg/Ca was found to be 2.35 for the 15-min sample, we surmise that the amorphous phase of the 15-min sample contains a substantial amount of Mg^{2+} ions. This observation is consistent with the FT-IR data which reveal the presence of magnesium salts in the 15-min sample. The Mg/Ca ratio decreases dramatically to 0.24 for the 40-min sample, whereas the Mg^{2+} ions incorporated in the precipitate increases to 14%. Apparently, a relatively large amount of Mg-calcite (1.6 mol % in Mg) has been precipitated in the 40-min sample, in addition to the Mg-rich amorphous phases. As the reaction times increases to 2 h, the Mg-rich amorphous phase redissolves into the supernatant so that the Mg^{2+} content of the supernatant increases. This process is accompanied by the formation of aragonite.

SEM and TEM. Figure 4 shows the SEM images of the 40-min, 2-h, and 24-h samples. For the 40-min sample, the major rock-like species are calcite crystallites and the minor worm-like species could be identified with the Mg-rich amorphous phase. For the 2-h sample, the XRD data have indicated the incipient formation of the aragonite phase. Accordingly, in the SEM image a significant amount of aragonite crystallites are found on the surface of calcite. At higher magnification, it is clearly shown that each "spicule" of the aragonite aggregate is formed by fusion of tiny crystallites of ca. 100 nm in size. Although the

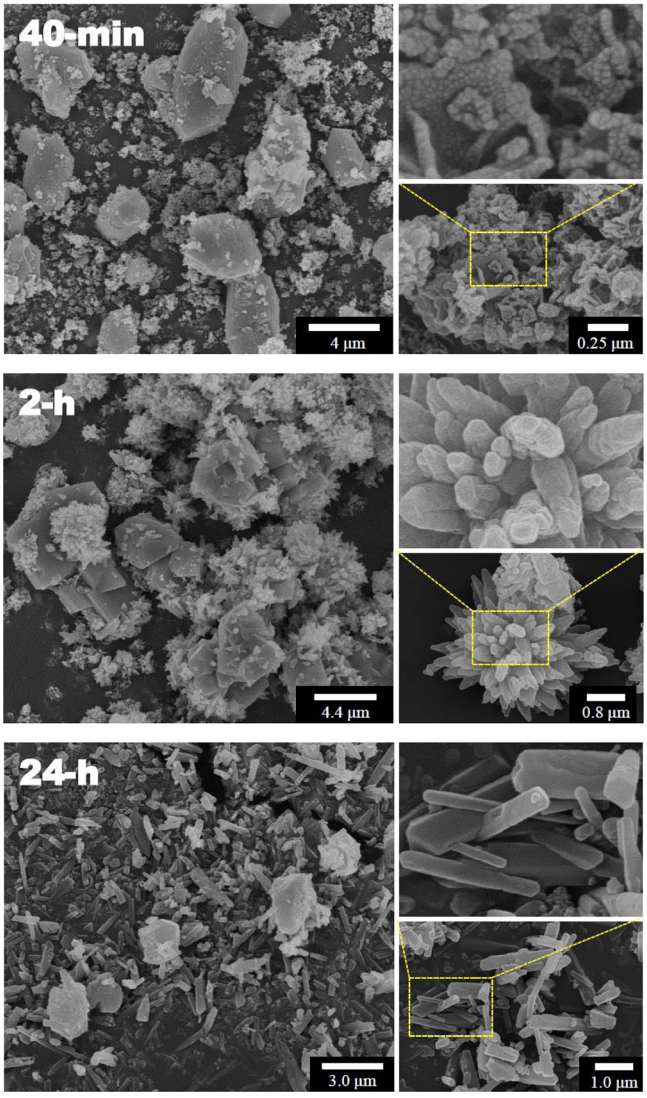

Figure 4. SEM images obtained for the 40-min, 2-h, and 24-h samples.

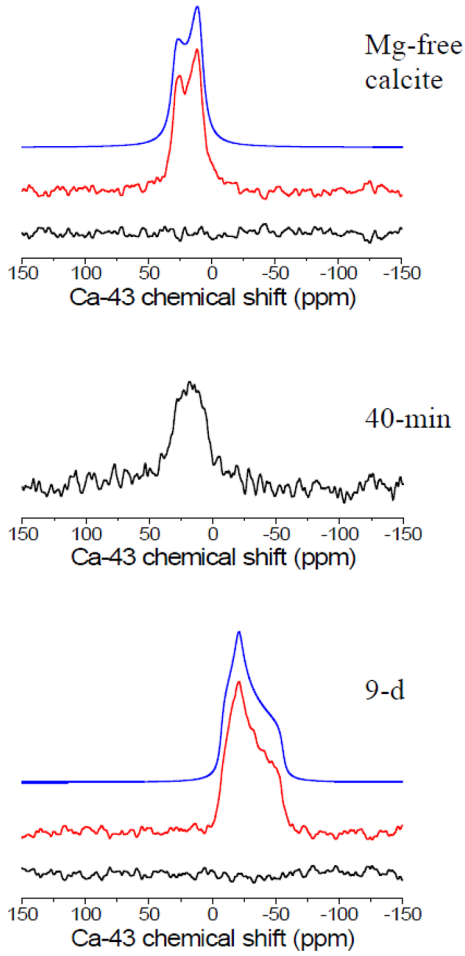

Figure 5. ^{43}Ca static spectra measured for the Mg-free calcite, 40-min, and 9-d samples (pure aragonite) using the Bloch-decay method. The upper, middle, and low traces represent the simulation, experimental, and the difference spectra, respectively. Sample (experimental conditions): Mg-free calcite (number of transients 1751, recycle delay 50 s), 40-min (5044, 50 s), and 9-d (6144, 25 s).

spicule was found to be polycrystalline by high-resolution TEM measurements (Figure S2), such linear fusion still implies some sort of structural ordering regarding to the relative orientation of two fused tiny crystallites. Otherwise, spherical or random aggregation would have been observed. As the reaction time increased to 24 h, the size of the calcite crystallites becomes smaller and the morphology of the aragonite crystallites becomes rod-like with sharp facets. For the 9-d sample, the samples are dominated by the rod like crystallites of aragonite (data not shown).

^{43}Ca NMR Data. On the basis of the XRD data, it has been shown that the calcium species of the 40-min sample exist mainly in the form of Mg-calcite, whereas the 9-d sample is pure aragonite. Recently, precise ^{43}Ca NMR data have been obtained for optical grade calcite. Figure 5 shows the static ^{43}Ca spectra of Mg-free calcite, the 40-min, and the 9-d samples. The experimental spectrum of Mg-free calcite and the one simulated based on the data reported in the literature are in favorable agreement.[22] However, the ^{43}Ca NMR signal of the 40-min sample is a featureless broad peak with the same chemical shift span as that of Mg-free calcite. Interestingly, the static spectrum of the 9-d sample can be simulated satisfactorily by considering the chemical shift anisotropy only. It suggests that the electric field gradient (EFG) at the calcium site must be relatively small. In other words, regarding the inhomogeneous broadening of the central transition, the effect of the chemical shift anisotropy is significantly larger than that of the second-order quadrupolar interaction. On the one hand, it helps simplify the spectral analysis of the static spectrum, so that measurements at multiple fields are not necessary. On the other hand, the characterization of the Euler angles relating the EFG and chemical shift tensors becomes very difficult. Inasmuch as the 2-h and 24-h samples contain two different phases of calcium carbonate, it may be difficult to deconvolute the static spectra of these samples. Nonetheless, under the high-resolution condition provided by MAS at 4 kHz, we can monitor the variation of the ^{43}Ca NMR parameters of the Mg-calcite and aragonite signals separately for the 2-h and 24-h samples.

Figure 6 shows the ^{43}Ca MAS spectra obtained for our sample series, where we include the spectrum of Mg-free calcite for comparison. The 15-min sample was not measured because of its very limited sample amount. As discussed in the foregoing sections, the 40-min, 2-h, and 24-h samples contain the crystalline phase of Mg-calcite. With reference to Figure 7, the corresponding Mg-calcite signals of the three samples invariably have two spectral components, viz., the major and minor one.

dx.doi.org/10.1021/jp309923p | J. Phys. Chem. B 2012, 116, 14295−14301

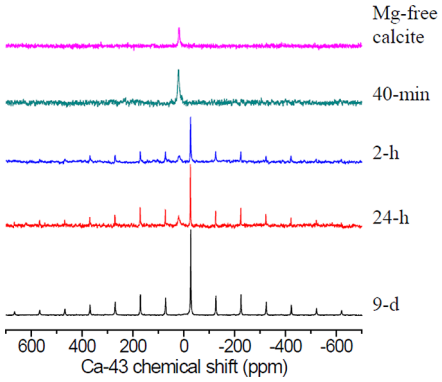

Figure 6. ^{43}Ca MAS spectra measured for the sample series using the Bloch-decay method. Samples (experimental conditions): Mg-free calcite (77.1 mg, number of transients 1048, ^{43}Ca enrichment 3%), 40-min (10.2 mg, 9811, 6%), 2-h (52.3 mg, 2509, 6%), 24-h (58.6 mg, 3105, 6%), and 9-d (44.0 mg, 5790, 6%).

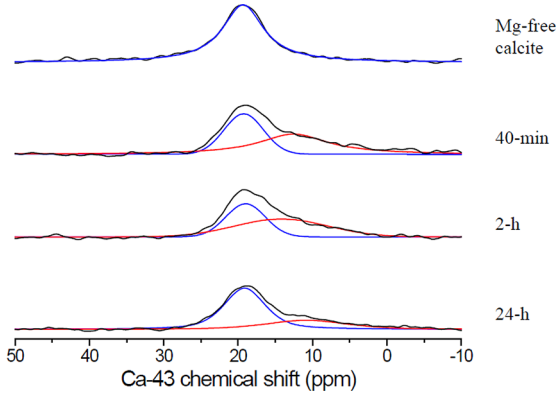

Figure 7. ^{43}Ca MAS spectra highlighting the signal region of calcite for the sample series. Spectra for Mg-free calcite and the 40-min sample are taken from Figure 6. The MAS spectra for the 2-h and 24-h samples were remeasured using the RAPT sequence with the number of transients equal to 1024 and 1560, respectively.

The major component has a very similar chemical shift and full width at half-maximum ($\Delta\nu_{1/2}$) to those of the Mg-free calcite (Table 1). It implies that the incorporation of Mg^{2+} ions in the calcitic lattice does not significantly perturb the electronic environment of most of the Ca^{2+} ions. This interpretation is reasonable because the amount of Mg^{2+} ions incorporated is 3% or less. Singer et al. also observed that the Ca^{2+} environment in ACC is not significantly affected by Mg^{2+} content.[39] The minor component resonates at 11 to 13 ppm and its $\Delta\nu_{1/2}$ is approximately two times larger than that of the major component. We believe that the minor component corresponds to the signal of the Ca^{2+} ions located near the surface of the crystallites, just as what has been suggested in the ^{17}O NMR study of nanocrystalline MgO.[40] Owing to the disordered nature of the surface signal, the static spectrum of the 40-min sample is rendered featureless (Figure 5). From the ^{43}Ca MAS spectrum obtained at a spinning frequency of 4 kHz, one can readily obtain the nuclear quadrupole coupling constant e^2qQ/h (C_Q) and the asymmetry parameter (η_Q) of the EFG at the ^{43}Ca site by simulating the spinning sideband intensities (Supporting Information). Note that the contribution of chemical shift anisotropy ($\delta_{zz} - \delta_{iso} = -1.1$ kHz) to the spinning sideband intensities has to be included to warrant satisfactory agreement between the experimental and simulated spectra. The ^{43}Ca NMR data including C_Q, η_Q, and chemical shift span and skew are summarized in Table 1, where it can be found that the ^{43}Ca quadrupolar parameters are very similar for the 2-h, 24-h, and 9-d samples. Indeed, the line widths of the center-band signals of the aragonite phase are also very similar. From the results of the ^{43}Ca saturation recovery experiments (Figure S5), the T_1 parameters extracted for the 2-h, 24-h, and 9-d samples were found to be 10.5 ± 2.2, 33.6 ± 3.4, and 33.4 ± 3.3 s, respectively. Because of the poor signal-to-noise ratio, we failed to characterize the T_1 parameter of the Mg-calcite phase. Therefore, we were not able to quantify the relative amount of the Mg-calcite and aragonite phases from the MAS spectra.

DISCUSSION

^{43}Ca NMR Parameters of Aragonite. The gauge-including projector augmented-wave (GIPAW) method, which is based on first-principles calculations with periodic boundary conditions, has been recently established as an important complementary tool to NMR in probing the structure of crystalline materials.[41,42] In particular, favorable agreement between the experimental and calculated ^{43}Ca NMR parameters of some interesting model crystalline compounds have also been reported.[22] In the field of biomineralization, however, the ^{43}Ca NMR studies of important crystalline model compounds remain relatively scarce in the literature. Among

Table 1. ^{43}Ca NMR Parameters for the Sample Series[a]

samples	assignment	%	δ_{iso} (ppm)	$\Delta\nu_{1/2}$ (Hz)	Ω (ppm)	κ	C_Q (kHz)	η_Q
Mg-free	calcite		19.3 ± 0.4	270				
40-min	Mg-calcite	63	19.0 ± 0.5	260				
		37	11 ± 1	510				
2-h	Mg-calcite	62	19.1 ± 0.1	260				
		38	13 ± 1	500				
	aragonite		−26.8 ± 0.2	87[b]			263 ± 3	0.5 ± 0.1
24-h	Mg-calcite	66	19.1 ± 0.3	265				
		33	11 ± 1	600				
	aragonite		−26.9 ± 0.1	80[b]			256 ± 3	0.35 ± 0.15
9-d	aragonite		−27.2 ± 0.1	84[b]	49.6 ± 0.5[c]	0.44 ± 0.01[c]	259 ± 3	0.35 ± 0.15
					52.2[d]	0.49[d]	320[d]	0.58[d]

[a]All data were extracted by analyzing the MAS spectra unless stated otherwise. δ_{iso}, isotropic chemical shift; Ω, chemical shift span; κ, chemical shift skew.[47] [b]Corresponding to the center band. [c]Data obtained by analyzing the static spectrum. [d]NMR data calculated using GIPAW by Bryce and co-workers.[22]

dx.doi.org/10.1021/jp309923p | J. Phys. Chem. B 2012, 116, 14295−14301

the studied compounds, only the results of apatite and calcite are well characterized. Therefore, more benchmark ^{43}Ca NMR experimental data for model compounds relevant to the studies of biominerals are in order. To date, the only available data for aragonite are the results reported for natural abundance sample at low field (8.46 T) by Dupree and co-workers.[26] In comparison, the data reported in this work provide a more accurate characterization of the chemical shift and quadrupolar interactions. Our extracted C_Q value for aragonite is smaller than that of calcite by an order of magnitude, which is consistent with the higher symmetry at the calcium site of aragonite.[43] The overall agreement between our experimental data and the GIPAW results[22] is very favorable for the chemical shift span and skew, whereas there is a considerable discrepancy in C_Q and η_Q. From a careful comparison of the experimental spinning sideband manifold and the one calculated based on the GIPAW results (Supporting Information), it is doubtless that the discrepancy cannot be accounted for by the random noise of the spectrum. Although we do not fully understand the origin of the discrepancy, we suggest that the crystal and/or molecular structures of our aragonite sample (9-d) may have some hitherto uncharacterized structural disorders, whereas the GIPAW calculations were based on the idealized structure.

Phase Transformation Mechanism. We have shown that the ^{43}Ca NMR parameters of the Mg-calcite are largely invariant among the sample series, from which we can conclude that the phase transformation from calcite to aragonite most likely would occur via the dissolution-reprecipitation pathway instead of solid-state transformation. The latter would presumably result in a detectable variation of ^{43}Ca chemical shifts during the phase transformation. From the AFM study of how Mg ions inhibit the crystal growth of calcite, it has been suggested that the Mg ions incorporated into the calcite lattice would enhance the mineral solubility.[44] Thus, the precipitation of Mg-calcite appears to be kinetically favored because of its lower surface free energy. As dissolution occurs, the ions near the surface of this polymorph become supersaturated with respect to the aragonite phase. After the onset of the nucleation process of aragonite at a later stage, the crystal growth of aragonite will take place at the expense of the Mg-calcite crystallites, just as what described in the process of Ostwald ripening. Indeed, we observe that the calcite and aragonite crystallites are in intimate proximity and that the calcite crystallites of the 24-h sample are smaller than those of the 2-h sample. Very recently, it has been reported that the ^{43}Ca NMR signal of ACC would appear at around 0 ppm with a line width of about 1.7 kHz at 20.0 T.[39] We do not find any evidence for the presence of the ACC phase in our samples, although we cannot completely rule out its presence in our samples.

Our ^{43}Ca NMR data have shed novel insight into the precipitation process of aragonite. Initially, the crystallites of aragonite appear as spine-like aggregates in the 2-h sample. Subsequently, the aggregates transform to rod-like crystallites in the 24-h sample. The XRD patterns and the ^{43}Ca quadrupolar parameters of the aragonite phase among the 2-h, 24-h, and 9-d samples are almost indistinguishable, reflecting a close resemblance in their molecular structure. Yet, the ^{43}Ca T_1 parameter of the 2-h sample is significantly shorter than those of the 24-h and 9-d samples. For our systems, it is legitimate to assume that the ^{43}Ca spin−lattice relaxation is dominated by the quadrupolar relaxation mechanism,[45] where the fluctuation of the EFG at the calcium site would induce the magnetic energy exchange between the ^{43}Ca spin system and the crystal lattice. Thus, the short ^{43}Ca T_1 parameter of the 2-h sample suggests that there are considerable motional dynamics of the lattice ions and that the time scale of motion is comparable to the inverse of the ^{43}Ca Larmor frequency.

When the growth and dissolution of subcritical nuclei are inhibited, the critical size of the nucleation center could be reached by aggregation of subcritical nuclei and the resultant crystallites become polycrystalline.[11] Because Mg^{2+} ions cannot enter the crystal lattice of aragonite, the polycrystalline nature of the "spicule" of the 2-h sample implies that the nucleation event of aragonite is regulated to certain extent by Mg^{2+} ions, although more experiments are required to corroborate this suggestion. The most important implication of our NMR data is that the difference in crystal morphologies of the aragonite phase in the 2-h and 24-h samples could be traced down to the subtle difference in motional dynamics at the molecular level. In view of the common occurrence of the nonclassical crystallization pathway in biominerals,[46] the aragonite phase in spine-like morphology seems to be more relevant to the biomineralization process. Such spine-like polymorph of aragonite also has relatively high surface free energy, so that it will gradually transform to the thermodynamically more stable rod like morphology via a local dissolution-reprecipitation process. Overall, our results show that ^{43}Ca spin−lattice relaxation parameters may be exploited to probe the difference between the crystallites with biogenic-like morphologies and their inorganic counterparts at the molecular level, which may open up new avenues for the ^{43}Ca SSNMR studies of calcified tissues.

■ CONCLUSIONS

^{43}Ca is an effective NMR probe nucleus for the study of phase transformation processes involving calcite and aragonite. In the presence of significant amount of Mg^{2+} ions, the system will transform to aragonite. Our ^{43}Ca solid-state NMR data support the dissolution-recrystallization mechanism for the calcite to aragonite transition. We find that the ^{43}Ca NMR parameters of Mg-calcite, which is an important biomineral phase, are very similar to those of pure calcite. Under the high-resolution condition provided by magic-angle spinning at 4 kHz, we can monitor the variation of the ^{43}Ca NMR parameters of the aragonite signals for the samples obtained at different reaction times. In particular, the ^{43}Ca C_Q and η_Q data of the aragonite phase of the 2-h and the 24-h samples are very similar to those of pure aragonite. On the contrary, the ^{43}Ca T_1 parameters were determined to increase dramatically as the reaction time increased from 2 to 24 h. The difference in crystal morphologies of the aragonite phase in the 2-h and 24-h samples has been traced down to the subtle difference in the motional dynamics at the molecular level, as inferred from the difference in the ^{43}Ca relaxation parameters.

■ ASSOCIATED CONTENT

Supporting Information

Sample amount collected at different reaction times, high-resolution XRD diffraction peaks of (104), high-resolution TEM images, deconvolution of the ^{43}Ca MAS spectra, and data of ^{43}Ca saturation recovery experiments. This material is available free of charge via the Internet at http://pubs.acs.org.

dx.doi.org/10.1021/jp309923p | J. Phys. Chem. B 2012, 116, 14295−14301

AUTHOR INFORMATION

Corresponding Author

*Phone: 886-2-33662994. Fax: 886-2-23636359. E-mail: chanjcc@ntu.edu.tw; shingjonghuang@ntu.edu.tw.

Notes

The authors declare no competing financial interest.

ACKNOWLEDGMENTS

This work was financially supported by the National Science Council (NSC 100-2628-M-002-009-MY3). The NMR measurements were carried out at the Instrumental Center of National Taiwan University (NSC-100-2731-M-002-002-MY2). The detailed comments of the reviewers are gratefully acknowledged.

REFERENCES

(1) Lowenstam, H. A.; Weiner, S. *On Biomineralization*; Oxford University Press: Oxford, U.K., 1989.
(2) Mann, S. *Biomineralization - Principles and Concepts in Bioinorganic Materials Chemistry*; Oxford University Press: New York, 2001.
(3) Fricke, M.; Volkmer, D. In *Biomineralization I*; Naka, K., Ed.; Springer: Berlin, 2007; Vol. *270*, p 1.
(4) Falini, G.; Gazzano, M.; Ripamonti, A. *Chem. Commun.* **1996**, 1037.
(5) Loste, E.; Wilson, R. M.; Seshadri, R.; Meldrum, F. C. *J. Cryst. Growth* **2003**, *254*, 206.
(6) Lenders, J. J. M.; Dey, A.; Bomans, P. H. H.; Spielmann, J.; Hendrix, M.; de With, G.; Meldrum, F. C.; Harder, S.; Sommerdijk, N. *J. Am. Chem. Soc.* **2011**.
(7) Han, Y. J.; Aizenberg, J. *J. Am. Chem. Soc.* **2003**, *125*, 4032.
(8) Liu, R.; Xu, X. R.; Cai, Y. R.; Cai, A. H.; Pan, H. H.; Tang, R. K.; Cho, K. *Cryst. Growth Des.* **2009**, *9*, 3095.
(9) Nishino, Y.; Oaki, Y.; Imai, H. *Cryst. Growth Des.* **2009**, *9*, 223.
(10) Cheng, X. G.; Varona, P. L.; Olszta, M. J.; Gower, L. B. *J. Cryst. Growth* **2007**, *307*, 395.
(11) Meldrum, F. C.; Hyde, S. T. *J. Cryst. Growth* **2001**, *231*, 544.
(12) Xie, A. J.; Shen, Y. H.; Li, X. Y.; Yuan, Z. W.; Qiu, L. G.; Zhang, C. Y.; Yang, Y. F. *Mater. Chem. Phys.* **2007**, *101*, 87.
(13) Park, W. K.; Ko, S. J.; Lee, S. W.; Cho, K. H.; Ahn, J. W.; Han, C. *J. Cryst. Growth* **2008**, *310*, 2593.
(14) Xiao, J. W.; Yang, S. H. *CrystEngComm* **2011**, *13*, 2472.
(15) Gervais, C.; Laurencin, D.; Wong, A.; Pourpoint, F.; Labram, J.; Woodward, B.; Howes, A. P.; Pike, K. J.; Dupree, R.; Mauri, F.; Bonhomme, C.; Smith, M. E. *Chem. Phys. Lett.* **2008**, *464*, 42.
(16) Laurencin, D.; Wong, A.; Dupree, R.; Smith, M. E. *Magn. Reson. Chem.* **2008**, *46*, 347.
(17) Laurencin, D.; Wong, A.; Hanna, J. V.; Dupree, R.; Smith, M. E. *J. Am. Chem. Soc.* **2008**, *130*, 2412.
(18) Pizzala, H.; Caldarelli, S.; Eon, J. G.; Rossi, A. M.; Laurencin, D.; Smith, M. E. *J. Am. Chem. Soc.* **2009**, *131*, 5145.
(19) Laurencin, D.; Almora-Barrios, N.; de Leeuw, N. H.; Gervais, C.; Bonhomme, C.; Mauri, F.; Chrzanowski, W.; Knowles, J. C.; Newport, R. J.; Wong, A.; Gan, Z.; Smith, M. E. *Biomaterials* **2011**, *32*, 1826.
(20) Laurencin, D.; Wong, A.; Chrzanowski, W.; Knowles, J. C.; Qiu, D.; Pickup, D. M.; Newport, R. J.; Gan, Z. H.; Duer, M. J.; Smith, M. E. *Phys. Chem. Chem. Phys.* **2010**, *12*, 1081.
(21) Xu, J. D.; Zhu, P. X.; Gan, Z. H.; Sahar, N.; Tecklenburg, M.; Morris, M. D.; Kohn, D. H.; Ramamoorthy, A. *J. Am. Chem. Soc.* **2010**, *132*, 11504.
(22) Bryce, D. L.; Bultz, E. B.; Aebi, D. *J. Am. Chem. Soc.* **2008**, *130*, 9282.
(23) Bryce, D. L. *Dalton Trans.* **2010**, *39*, 8593.
(24) Hanna, J. V.; Smith, M. E. *Solid State Nucl. Magn. Reson.* **2010**, *38*, 1.
(25) Bryant, R. G.; Ganapathy, S.; Kennedy, S. D. *J. Magn. Reson.* **1987**, *72*, 376.
(26) Dupree, R.; Howes, A. P.; Kohn, S. C. *Chem. Phys. Lett.* **1997**, *276*, 399.
(27) Lin, Z. J.; Smith, M. E.; Sowrey, F. E.; Newport, R. J. *Phys. Rev. B* **2004**, *69*, 7.
(28) MacKenzie, K. J. D.; Rahner, N.; Smith, M. E.; Wong, A. *J. Mater. Sci.* **2010**, *45*, 999.
(29) Moudrakovski, I. L.; Alizadeh, R.; Beaudoin, J. J. *Phys. Chem. Chem. Phys.* **2010**, *12*, 6961.
(30) Bowers, G. M.; Kirkpatrick, R. J. *Cryst. Growth Des.* **2011**, *11*, 5188.
(31) MacDonald, J. L.; Werner-Zwanziger, U.; Chen, B.; Zwanziger, J. W.; Forgeron, D. *Solid State Nucl. Magn. Reson.* **2011**, *40*, 78.
(32) Wong, A.; Aguiar, P. M.; Charpentier, T.; Sakellariou, D. *Chem. Sci.* **2011**, *2*, 815.
(33) Yao, Z.; Kwak, H. T.; Sakellariou, D.; Emsley, L.; Grandinetti, P. J. *Chem. Phys. Lett.* **2000**, *327*, 85.
(34) Siegel, R.; Nakashima, T. T.; Wasylishen, R. E. *Concept Magn. Reson. A* **2005**, *26A*, 47.
(35) Massiot, D.; Fayon, F.; Capron, M.; King, I.; Le Calve, S.; Alonso, B.; Durand, J. O.; Bujoli, B.; Gan, Z. H.; Hoatson, G. *Magn. Reson. Chem.* **2002**, *40*, 70.
(36) Michel, F. M.; MacDonald, J.; Feng, J.; Phillips, B. L.; Ehm, L.; Tarabrella, C.; Parise, J. B.; Reeder, R. J. *Chem. Mater.* **2008**, *20*, 4720.
(37) Tao, J.; Zhou, D.; Zhang, Z.; Xu, X.; Tang, R. *Proc. Natl. Acad. Sci. U.S.A.* **2009**, *106*, 22096.
(38) Radha, A. V.; Forbes, T. Z.; Killian, C. E.; Gilbert, P. U. P. A.; Navrotsky, A. *Proc. Natl. Acad. Sci. U.S.A.* **2010**, *107*, 16438.
(39) Singer, J. W.; Yazaydin, Z. O.; Kirkpatrick, R. J.; Bowers, G. M. *Chem. Mater.* **2012**, *24*, 1828.
(40) Chadwick, A. V.; Poplett, I. J. F.; Maitland, D. T. S.; Smith, M. E. *Chem. Mater.* **1998**, *10*, 864.
(41) Ashbrook, S. E. *Phys. Chem. Chem. Phys.* **2009**, *11*, 6892.
(42) Charpentier, T. *Solid State Nucl. Magn. Reson.* **2011**, *40*, 1.
(43) Dickens, B.; Bowen, J. *J. Res. Nat. Bur. Stand., Sec. A* **1971**, *A 75*, 27.
(44) Davis, K. J.; Dove, P. M.; De Yoreo, J. J. *Science* **2000**, *290*, 1134.
(45) Freude, D.; Haase, J. In *NMR Basic Principles and Progress*; Diehl, P., Fluck, E., Gunther, H., Kosfeld, R. S. J., Eds.; Springer: Berlin, 1993; Vol *29*, p 1.
(46) Meldrum, F. C.; Colfen, H. *Chem. Rev.* **2008**, *108*, 4332.
(47) Mason, J. *Solid State Nucl. Magn. Reson.* **1993**, *2*, 285.